miR-33a promotes glioma-initiating cell self-renewal via PKA and NOTCH pathways

Hui Wang,[1] Tao Sun,[1] Jing Hu,[1] Rui Zhang,[2] Yanhua Rao,[1] Shuai Wang,[3] Rui Chen,[1] Roger E. McLendon,[4] Allan H. Friedman,[4] Stephen T. Keir,[4] Darell D. Bigner,[4] Qi-Jing Li,[5] Huibo Wang,[2] and Xiao-Fan Wang[1]

[1]Department of Pharmacology and Cancer Biology, Duke University Medical Center, Durham, North Carolina, USA. [2]Department of Neurosurgery and [3]Department of Hematology, The First Affiliated Hospital of Nanjing Medical University, Nanjing, China. [4]The Preston Robert Tisch Brain Tumor Center and [5]Department of Immunology, Duke University Medical Center, Durham, North Carolina, USA.

Glioblastoma (GBM) is the most common and lethal brain tumor in adults. Glioma-initiating cells (GICs) are stem-like cells that have been implicated in glioblastoma progression and recurrence; however, the distinct properties of GICs and non-GICs within GBM tumors are largely uncharacterized. Here, we evaluated stem cell–associated microRNA (miR) expression in GICs from GBM patients and GICs derived from xenografted human glioma cell lines and determined that miR-33a promotes GIC growth and self-renewal. Moreover, evaluation of a GBM tissue array revealed that higher miR-33a expression was associated with poor prognosis of GBM patients. Antagonizing miR-33a function in GICs reduced self-renewal and tumor progression in immune-compromised mice, whereas overexpression of miR-33a in non-GICs promoted the display of features associated with GICs. We identified the mRNAs encoding phosphodiesterase 8A (PDE8A) and UV radiation resistance–associated gene (UVRAG) as direct miR-33a targets. PDE8A and UVRAG negatively regulated the cAMP/PKA and NOTCH pathways, respectively; therefore, miR-33a–dependent reduction of these proteins promoted growth and self-renewal of GICs by enhancing PKA and NOTCH activity. Furthermore, in GBM specimens, there was an inverse correlation between the expression levels of miR-33a and *PDE8A* and *UVRAG* expression. These findings reveal a miR-33a–centered signaling network that promotes GIC maintenance and has potential as a therapeutic target for GBM treatment.

Introduction

Glioblastoma (GBM, WHO grade IV astrocytoma) is the most common and lethal primary brain tumor in adults, with an average survival of slightly more than one year after initial diagnosis (1). GBMs exhibit significant heterogeneity within the tumor mass, in which a subpopulation of cells named tumor-initiating cells (TIC) or cancer stem cells possess potent tumorigenic ability when they are implanted in immune-deficient mice (2). Those glioma-initiating cells (GICs) display stem cell–like characteristics that are normally associated with neural stem cells (NSCs), including self-renewal demonstrated by their ability to form neurospheres in culture during serial dissociations and passages, expression of NSC markers (e.g., cell-surface antigen CD133, transcription factors nestin and OLIG2), and potential to differentiate into multiple lineages, such as neurons, astrocytes, and oligodendroglia (3). GICs have also been shown to account for resistance to radio- and chemotherapies (4, 5). These biological properties of GICs are considered to be crucial for GBM occurrence and recurrence; however, the molecular mechanisms underlying the functional differences between GICs and non-GICs within the GBM tumor mass remain largely unknown.

MicroRNAs (miRNAs) are a class of noncoding small RNA molecules, typically about 18–22 nucleotides in the mature form (6). miRNAs negatively regulate gene expression at the posttranscriptional level by promoting mRNA degradation and/or inhibiting mRNA translation. miRNAs in theory could be involved in almost every aspect of biological processes by targeting about one-third of protein-coding genes in the human genome (7). In recent years, a large number of miRNAs have been found to be deregulated in many types of cancer: some function as tumor promoters and others as tumor suppressors (8). For example, among the most extensively studied miRNAs, the miR17–92 clusters and miR-21 are reported to function as onco-mirs in a variety of tumors through multiple mechanisms (9–11). In the context of GBM, particularly GICs, the critical roles of miRNAs in defining the functions of GICs have just started to be appreciated (12, 13), with details of mechanisms remaining to be fully explored.

Here, we report the identification of miR-33a as an essential miRNA to maintain GIC growth and self-renewal. miR-33a exhibits an elevated level of expression in GICs compared with non-GICs, and a correlation is detected in GBM patients between higher expression of miR-33a and poor prognosis. Antagonism of miR-33a activity in $CD133^+$ GICs from xenograft lines led to loss of self-renewal capability, measured by decreased ability to form neurospheres and reduced expression of stemness markers. Furthermore, $CD133^+$ GICs from xenograft lines with suppressed miR-33a function displayed compromised ability to generate intracranial tumors in nude mice. Importantly, overexpression of miR-33a in $CD133^-$ non-GICs from xenograft lines appeared to reprogram those cells into a state resembling GICs, as demonstrat-

Authorship note: Hui Wang, Tao Sun, and Jing Hu contributed equally to this work.
Note regarding evaluation of this manuscript: Manuscripts authored by scientists associated with Duke University, The University of North Carolina at Chapel Hill, Duke-NUS, and the Sanford-Burnham Medical Research Institute are handled not by members of the editorial board but rather by the science editors, who consult with selected external editors and reviewers.
Conflict of interest: The authors have declared that no conflict of interest exists.
Submitted: January 21, 2014; **Accepted:** August 7, 2014.
Reference information: *J Clin Invest*. 2014;124(10):4489–4502. doi:10.1172/JCI75284.

ed by their enhanced ability to form neurospheres associated with an increased expression of stemness markers as well as a potent augmentation in the formation of xenograft tumors. Mechanistically, we have identified several downstream targets of miR-33a that could contribute to the functional effect of this miRNA on the biological activity of GICs. Among them, phosphodiesterase 8A (PDE8A) is a negative regulator of the cAMP/PKA pathway that has not previously been implicated as involved in the biology of TICs. Another target of miR-33a, UV radiation resistance–associated gene (UVRAG), can negatively modulate the activity of the NOTCH pathway. Repression of PDE8A and UVRAG by miR-33a or antagonists of the PKA or NOTCH pathways could potently affect the growth and self-renewal of the $CD133^+$ GICs from xenograft lines. Furthermore, the expression level of these 2 targets of miR-33a displays a reverse correlation with that of miR-33a in GBM patient samples, strongly supporting the clinical importance of the newly identified signaling network. Finally, blockage of miR-33a activity by modified small RNA antagonists strongly inhibited GIC-initiated tumor progression in a subcutaneous GBM model, suggesting that the miR-33a–mediated signaling network could serve as a promising therapeutic target for the treatment of GBM.

Results

Identification of miR-33a as an onco-mir with higher expression in GICs correlated with poor prognosis of glioma patients. To identify miRNAs that may contribute to the biological properties that distinguish GICs from non-GICs, we conducted a candidate-based screen of miRNAs that are known through previous studies to be involved in regulating stem cell biology. We employed 2 established experimental procedures to enrich GICs. For the first procedure, we used the cell-surface marker CD133 to isolate GICs from patient-derived glioma lines maintained through serial passage in athymic BALB/c nu/nu mice as subcutaneous xenografts that possess many features of the parental tumors even after a long series of passages. With this method, 5% to 15% of the tumor cells were found to be $CD133^+$ from 2 glioma lines, D456MG and 11-0040, with the percentage of those cells increased modestly along with passage number of the xenografted tumors (Supplemental Figure 1, A and B; supplemental material available online with this article; doi:10.1172/JCI75284DS1). These results are consistent with previous findings that proportion of $CD133^+$ cells ranged from 3% to 29% in glioma patient samples (2, 5). Importantly, differences in the ability of those isolated $CD133^+$ cells to form neurospheres and intracranial tumors were clearly observed when limited number of cells were tested (Supplemental Figure 1, C–F), strongly indicating that this approach is valid for the isolation of GICs. For the second procedure, we utilized a specific culturing condition that could significantly enrich the cell population that displayed biological properties of GICs but contained both $CD133^+$ and $CD133^-$ GICs (14). With this method, using freshly collected patient specimens, we measured the expression levels of stemness markers (nestin, *OLIG2*, and *BMI1*) by reverse-transcription PCR (RT-PCR) in 12 tumor samples, since we could not obtain a sufficient number of cells from each sample to conduct in vivo functional assays. As shown in Supplemental Figure 2, these stemness markers displayed higher expression in GICs enriched by the selective medium. Although both methods can enrich GICs from dissociated glioma cells, it is likely that certain percentage of GICs remain in the so-called "non-GIC" category. Despite the impurity of the non-GICs, the 2 populations of glioma cells display clearly distinctive biological properties that would form the basis of our functional assays employed in this study.

Subsequently, we used 3 freshly isolated GBM patient specimens and 3 xenografted glioma lines for the initial screen. The expression profiles of 80 miRNAs in the GICs and non-GICs isolated from those 6 tumor samples were determined, and those miRNAs that displayed significant differences in their expression levels between the 2 subpopulations of cells are shown in Supplemental Table 1. All together, 14 miRNAs were found upregulated and 2 miRNAs downregulated, with these changes common in all 6 tumor samples (results from this miRNA array are summarized in Supplemental Table 2). In this group, miR-101 and miR-181a were recently identified as exhibiting differential expression profiles in $CD133^+$ glioma cells by a similar screening (12), providing support to the reliability of our expression profiling. Interestingly, 6 of the 14 upregulated miRNAs belong to the miR-17–92 cluster family, members of which have been extensively studied and defined as onco-mirs in other cancer types (9, 15).

To assess the potential function of these miRNAs, we successfully individually overexpressed 4 of the 6 remaining upregulated miRNAs with less-known functions in $CD133^+$ D456MG cells and assessed whether they could affect the formation of neurospheres, as we were mostly interested in those miRNAs involved in the control of GIC properties associated with stemness. In this assay, miR-33a, while not exhibiting the most significant change in the expression level between the 2 populations of glioma cells (Supplemental Table 2), emerged as the top candidate due to its potent positive effect on neurosphere formation, which is in contrast to the other 3 miRNAs, which did not display any significant effects on neurosphere formation of GICs in comparison with controls (Supplemental Figure 3). Although this miRNA has never been studied in the context of cancer, previous reports indicated that miR-33a could act as an important regulator of cholesterol and fatty acid homeostasis via repression of key genes in cholesterol export, high-density lipoprotein metabolism, fatty acid oxidation, and glucose metabolism (16–18). To further assess the expression pattern of miR-33a in GBM, we collected more than 50 fresh patient specimens from the Duke Brain Tumor Center and were able to cultivate and isolate a sufficient number of cells from 16 samples to conduct validation experiments. As illustrated in Figure 1A, the expression level of miR-33a was significantly elevated in GICs enriched by selective medium compared with their corresponding non-GICs derived from the same tumor samples. In the meantime, we also examined miR-33a expression patterns in GICs enriched by the CD133 marker from 3 different patient-derived xenograft glioma lines, as they would be used in the majority of the subsequent experiments. As an alternative to CD133 as a marker to enrich GICs, we utilized another cell surface-marker, stage-specific embryonic antigen 1 (SSEA-1), which is also commonly used for this purpose (19, 20). Consistent with the results generated from freshly isolated GBM specimens, miR-33a is highly expressed in the GIC population, enriched by both CD133 and SSEA-1 (Figure 1, B and C). These results indicate that higher levels of miR-33a expression could be a common molecular signature of GICs in

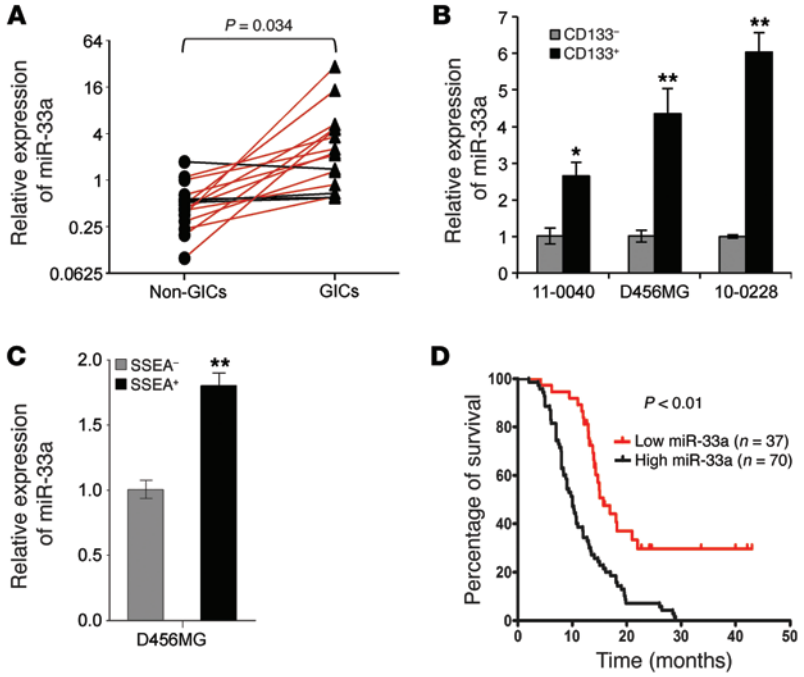

Figure 1. Identification of miR-33a as a top candidate among those differentially expressed miRNAs between GICs and non-GICs isolated from fresh GBM patient specimens and xenografts. (**A**) A scatter dot plot shows the expression pattern of miR-33a in GICs enriched by defined medium compared with their non-GIC counterparts in 16 clinical GBM specimens, as detected by qRT-PCR. *RNU6* was used as an internal control. (**B**) Relative expression levels of miR-33a in GICs enriched by CD133⁺selection from 3 xenograft tumor lines compared with their CD133⁻ counterparts, as detected by qRT-PCR. *RNU6* was used as an internal control. (**C**) Expression levels of miR-33a were examined by qRT-PCR in the SSEA-1–positive versus SSEA-1–negative cells isolated from D456MG through flow cytometry. (**D**) The ISH analysis of miR-33a was performed on 107 human GBM tumor tissues, and correlation between miR-33a levels and overall patient survival was shown by the Kaplan-Meier curve, with high (n = 70) or low (n = 37) miR-33a expression. *P < 0.05; **P < 0.01.

comparison with non-GICs. Importantly, we conducted ISH analyses on tissue microarrays (TMAs) from 107 GBM patient specimens and demonstrated that higher levels of miR-33a expression were correlated with poor survival of GBM patients (Figure 1D). A similar correlation was also found from analyses of The Cancer Genome Atlas database (https://tcga-data.nci.nih.gov/tcga/) on gliomas (data not shown). Together, these data strongly suggest that miR-33a acts as an onco-mir in the context of GBM, probably by exerting its affect on the function of GICs.

To explore the potential mechanism associated with elevated levels of miR-33a in GICs, we examined the expression pattern of *SREBP2*, which is the host gene of miR-33a with a single promoter (16), and found a similarly elevated level of SREBP2 in the CD133⁺ GICs compared with the CD133⁻ non-GICs isolated from D456MG and 11-0040 glioma xenografts (Supplemental Figure 4, A and B). Further analysis on the methylation status of the *SREBP2*/miR-33a promoter revealed a potential link between the hypomethylation of multiple CpG islands and higher levels of *SREBP2* mRNA/miR-33a in the CD133⁺ GICs in comparison with the CD133⁻ non-GICs (Supplemental Figure 4, C and D), suggesting that differential expression of miR-33a in the 2 populations of glioma cells might be determined at the transcriptional level.

Inhibition of miR-33a suppressed self-renewal and tumor-initiation abilities of GICs. To determine the role of endogenous miR-33a in GICs, we employed 2 different methods to antagonize the function of miR-33a. First, we generated a lentiviral-based sponge construct to attenuate the function of miR-33a (33a-sponge) to examine its effects in GICs. Then we verified the results using a miRZIP method that antagonizes miR-33a by expressing a miR-33a antisense RNA. It has been shown before that a miRNA sponge can cause a significant and specific reduction in the level of mature miRNA (21), so we used quantitative RT-PCR (qRT-PCR) to measure the mature miR-33a level and showed a robust knockdown efficiency of miR-33a (Supplemental Figure 5, A and B). Using the neurosphere formation assay, we found that attenuating the function of miR-33a in CD133⁺ GICs led to a significant decrease in their ability to form neurospheres (Figure 2A and Supplemental Figure 6, A, D, and G). Similar results were observed in GICs enriched by the marker SSEA-1 (Supplemental Figure 6F). Inhibition of miR-33a also resulted in a decrease in the expression of stemness markers nestin, *OLIG2*, and *BMI1* (Figure 2B and Supplemental Figure 6B). In addition, CD133⁺ D456MG cells from the miR-33a–sponge group displayed a slightly decreased proliferation rate (Supplemental Figure 7A), whereas the activity of apoptosis or multilineage differentiation was not altered (Supplemental Figure 7, B–E). To provide further support to the notion that miR-33a expression is correlated with stemness in the context of neural stem cells (NSCs), we compared the relative expression levels of miR-33a in the embryonic stem cell–derived H9 NSCs and D456MG-derived CD133⁺ and CD133⁻ cells. As shown in Supplemental Figure 8, A and B, miR-33a was present at the highest levels in the H9 NSCs, and knockdown of its expression led to a significant downregulation in the expression of several stemness markers. We also tested whether miR-33a could play a role during the transformation process with the introduction of glioma-inducing genetic mutations into normal human astrocytes, which could generate intracranial tumors resembling poorly differentiated high-grade glioma (22, 23). Interestingly, the fully transformed astrocytes expressed a higher level of miR-33a in comparison with the untransformed counterparts (Supplemental Figure 8C). Similar to the GICs isolated from GBM patients, these cells could proliferate and generate neurosphere-like cell aggregates when cultured in the serum-free medium supplemented with growth factors, indicating that they had acquired the ability of self-renewal (Supplemental Figure 8D). Importantly, blockage of miR-33a negatively affected the ability of the transformed astrocytes to form neurospheres (Supplemental Figure 8D), suggesting that miR-33a acts in a manner similar to that in patient-derived GICs. Finally, to determine the potential

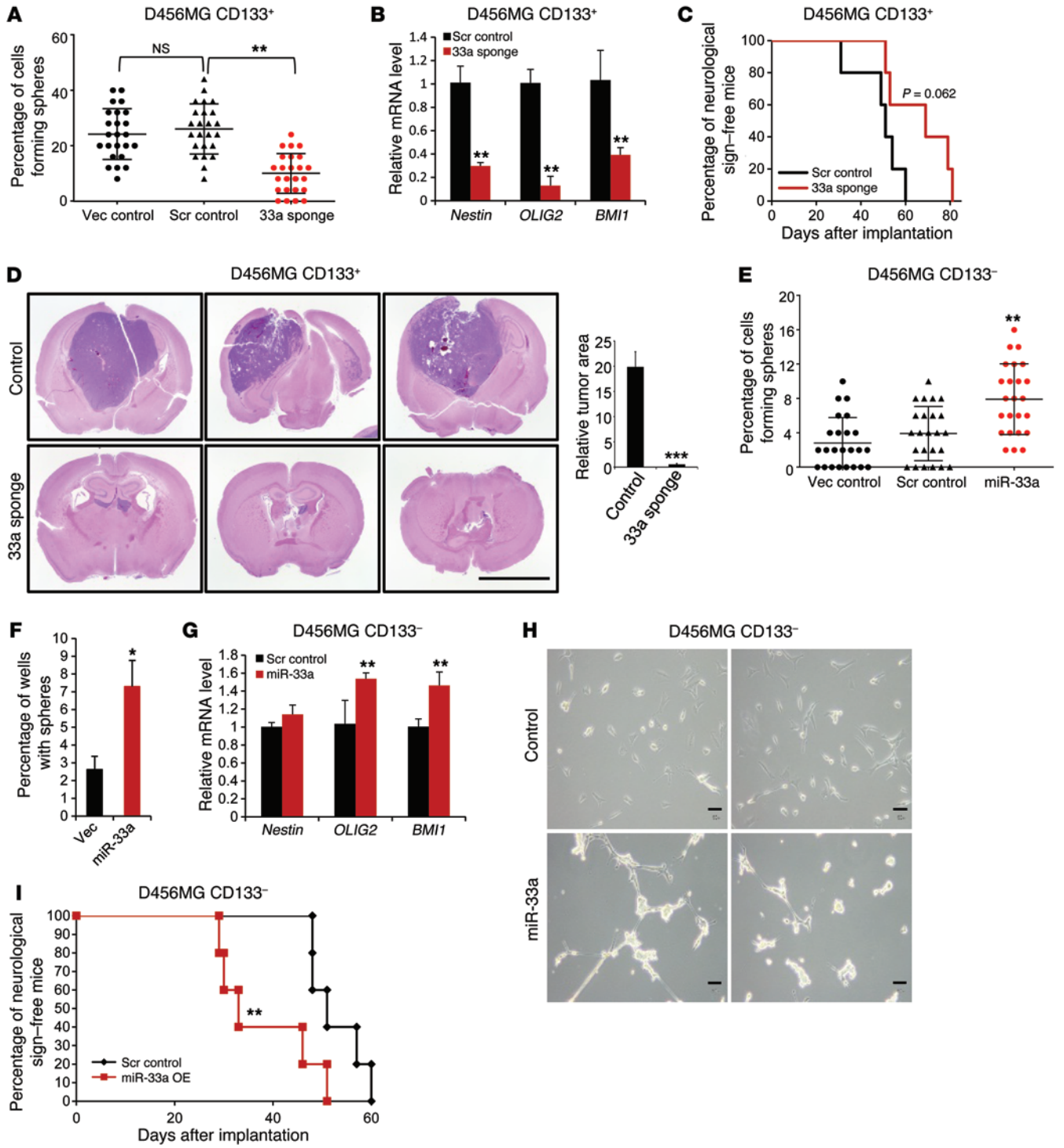

Figure 2. miR-33a promotes self-renewal and tumor progression of GICs. (**A**) Neurosphere formation assay was performed for CD133+ D456MG cells expressing indicated plasmids. Vec, vector; Scr, scramble. (**B**) qRT-PCR analysis was performed to determine the expression pattern of indicated stemness-associated genes in CD133+ D456MG cells expressing miR-33a sponge. (**C**) Kaplan-Meier curves were drawn to measure the burden of tumor progression by CD133+ D456MG cells expressing control or miR-33a sponge. 5,000 cells were implanted respectively in each mouse. $n = 5$. (**D**) H&E staining of brain sections indicating intracranial tumors formed 30 days after inoculation of 5,000 CD133+ D456MG cells expressing control or miR-33a sponge. Pictures were taken at the maximum cross section of tumors from each brain. Tumor areas were quantified using ImageJ (http://imagej.nih.gov/ij/). $n = 3$. Scale bar: 5.0 mm. (**E**) Neurosphere formation assay of CD133− D456MG cells with miR-33a overexpression compared with controls. (**F**) Single CD133− D456MG cells with miR-33a overexpression or control were plated into 96-well plates, and percentage of wells with a neurosphere was calculated 10 days later. (**G**) qRT-PCR analysis was performed to determine the expression pattern of indicated stemness-associated genes in CD133− D456MG cells overexpressing miR-33a. (**H**) Representative pictures of CD133− D456MG cells overexpressing miR-33a. Scale bar: 50 μm. (**I**) Kaplan-Meier curves were drawn to measure the burden of tumor progression by CD133− D456MG cells expressing scramble control or miR-33a. 100,000 cells were implanted in each mouse. $n = 5$. For neurosphere formation assays, 50 cells were plated in each well of 24-well plates. For qRT-PCR assays, *ACTB* was used as an internal control. $^*P < 0.05$; $^{**}P < 0.01$; $^{***}P < 0.001$.

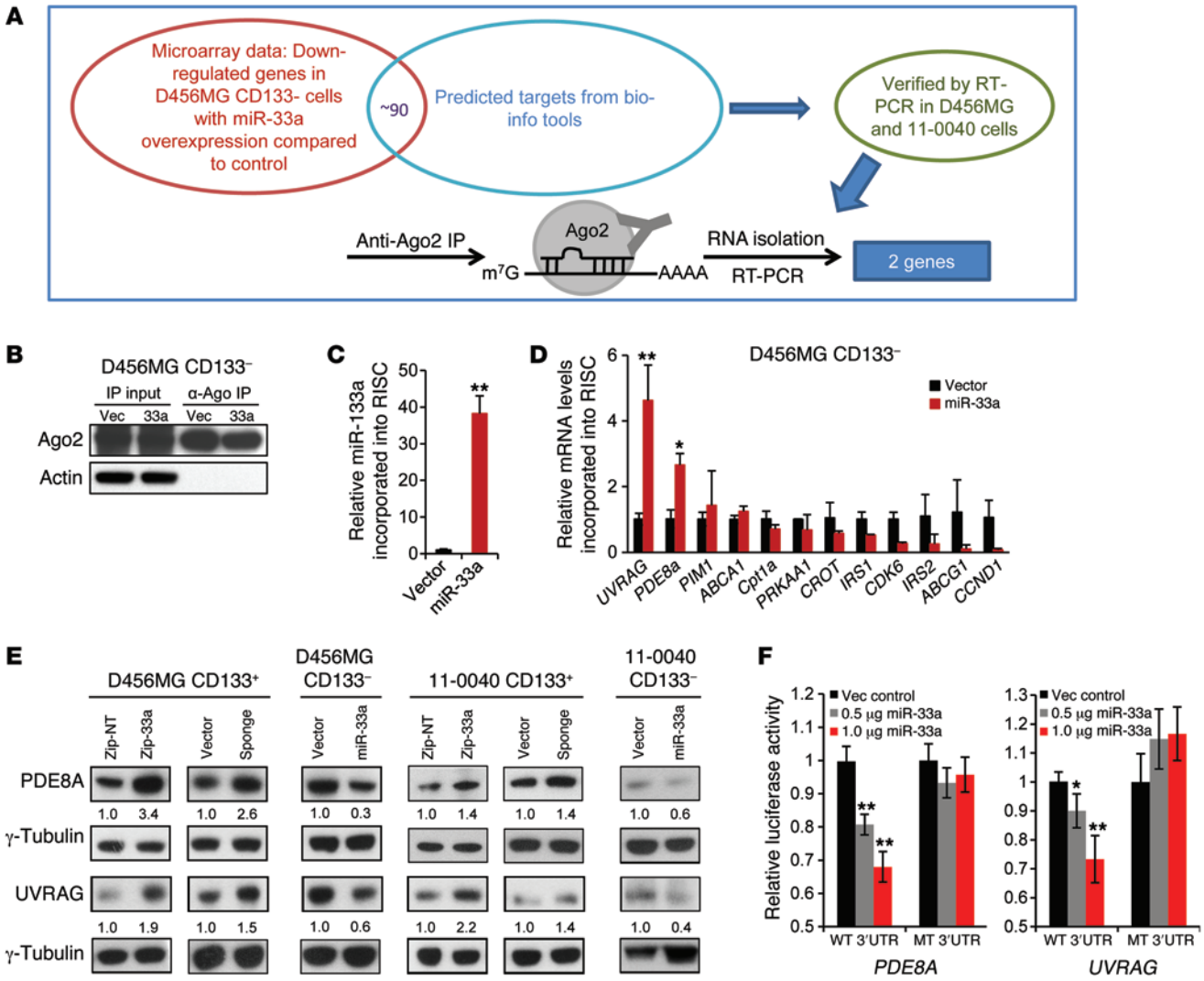

Figure 3. *PDE8A* and *UVRAG* are direct targets of miR-33a in glioma cells. (**A**) An illustration of strategies to identify direct targets of miR-33a. (**B**) RNA-Ago2 immunoprecipitation (IP) using lysates from D456MG CD133⁻ cells expressing the vector control or miR-33a as indicated. β-Actin was used as the loading control. (**C**) qRT-PCR analysis was performed to measure miR-33a levels incorporated into RISC in miR-33a–overexpressing cells compared with those of the control. *RNU6* was used as an internal control. (**D**) qRT-PCR analysis was performed to measure the levels of indicated mRNAs incorporated into RISC derived from miR-33a–overexpressing or vector control cells. *ACTB* was used as an internal control. (**E**) Immunoblotting was performed to show PDE8A and UVRAG protein levels in D456MG and 11-0040 cells as indicated, with repression (miRZIP) or sponge as marked) or overexpression of miR-33a. Intensities of bands were quantified using Image J and γ-tubulin was used as internal control to calculate the fold-change. (**F**) Luciferase activity of the reporter construct containing the wild type or miR-33a–binding mutant 3′ UTR of *PDE8A* or *UVRAG* was measured after cotransfection with control, or 0.5 μg or 1 μg miR-33a–expressing construct, respectively, in 293FT cells. $^*P < 0.05$; $^{**}P < 0.01$ compared with control group.

impact of suppressing miR-33a in vivo, we injected equal numbers of viable CD133⁺ GICs into nude mice to evaluate tumor initiation and progression. Consistent with the effect on the CD133⁺ GICs in culture, antagonizing miR-33a's function dramatically slowed GBM progression in mice bearing intracranial xenograft tumors, as shown in Figure 2C and Supplemental Figure 6, C, E, and H. In another experimental setting, we inoculated equal numbers of viable CD133⁺ GICs intracranially into nude mice and sacrificed the mice from both the control and miR-33a–knockdown group on the same day, when the first mouse in the control group developed neurological signs due to tumor growth. Histological analysis by H&E staining revealed a significantly smaller tumor area in the miR-33a–knockdown group (Figure 2D and Supplemental Figure 6I). All of these experiments were performed in GICs from 2 different patient-derived xenograft glioma lines and obtained consistent results. In sum, these data demonstrate that miR-33a expression was critical for the ability of CD133⁺ GICs and cells transformed from normal human astrocytes to maintain their self-renewal in culture and CD133⁺ GICs to generate tumors in vivo.

Overexpression of miR-33a rendered CD133⁻ non-GICs to behave like CD133⁺ GICs. The effects of suppressing miR-33a in GICs on self-renewal prompted us to determine whether miR-33a is also sufficient to confer the phenotype on CD133⁻ non-GICs. To test this possibility, we introduced miR-33a into CD133⁻ glioma cells via a lentiviral vector that also expressed a GFP selection marker to allow isolation of transduced cells by FACS. The ectopic expres-

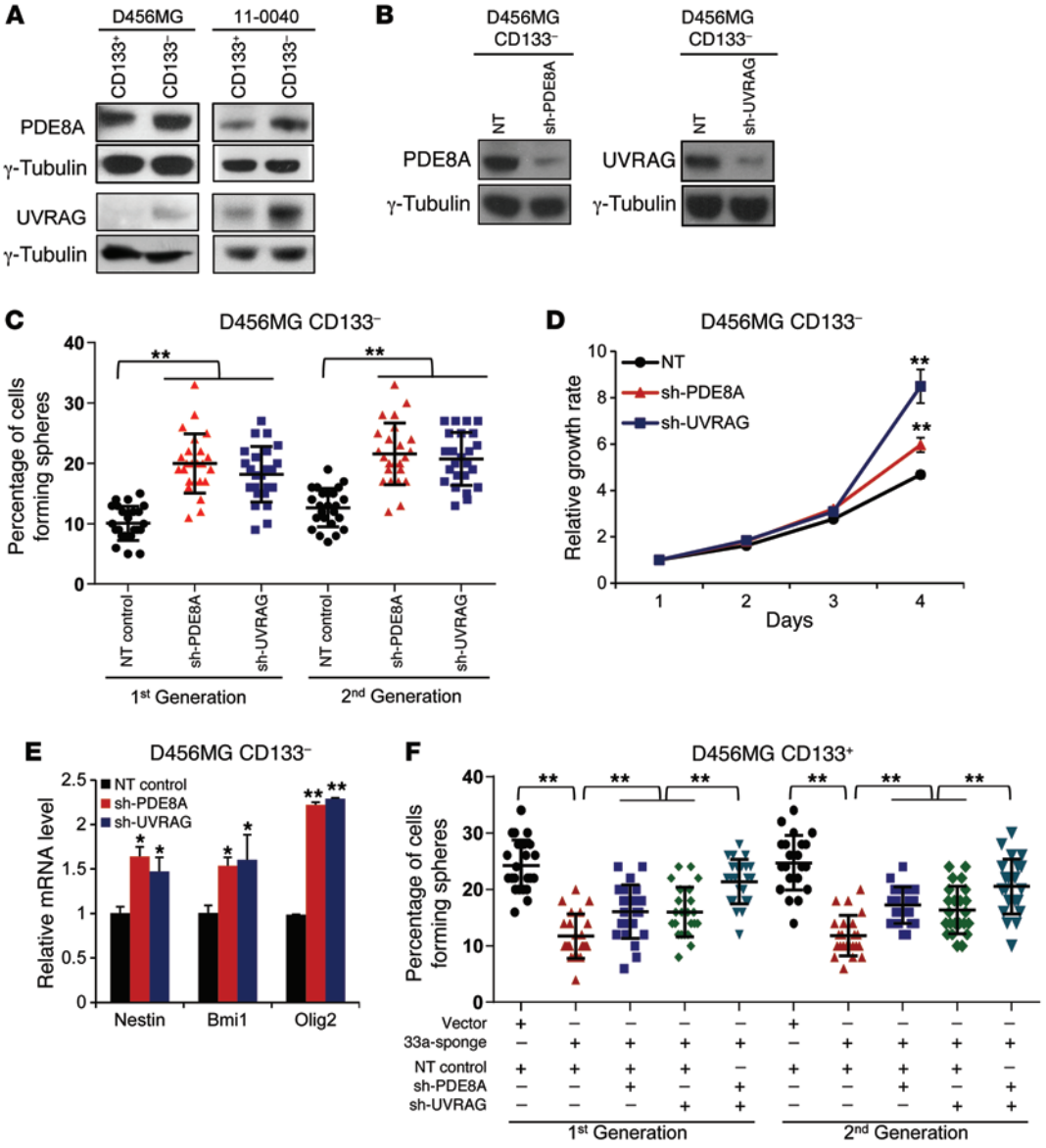

Figure 4. Repression of PDE8A and UVRAG expression is required for the function of miR-33a in glioma cells. (**A**) Protein levels of PDE8A and UVRAG were measured by immunoblots in CD133+ and CD133− D456MG and 11-0040 cells. γ-Tubulin was used as internal control. (**B**) Protein levels of PDE8A and UVRAG were measured by immunoblots in shRNA-mediated knockdown of the 2 genes in CD133− D456MG cells. γ-Tubulin was used as internal control. (**C**) Neurosphere formation assay was performed in CD-133− D456MG cells with PDE8A and UVRAG knockdown, respectively. 100 cells were plated in each well of 24-well plates. (**D**) Growth rate of CD133− D456MG cells with PDE8A and UVRAG knockdown or vector control was measured by cell titer assay. (**E**) qRT-PCR analysis was performed to determine the expression levels of stemness-associated genes in CD133− D456MG cells with PDE8A and UVRAG knockdown or scramble control. *ACTB* was used as an internal control. (**F**) Neurosphere formation assays were performed in CD133+ D456MG cells expressing miR-33a sponge or vector control with stable PDE8A and UVRAG knockdown or scramble control as indicated. NT control, nontargeting control. $^{*}P < 0.05$; $^{**}P < 0.01$.

sion level of miR-33a in CD133− non-GICs was physiologically relevant, within a range of expression levels similar to the endogenous miR-33a level in CD133+ cells isolated from the same tumor sample (Supplemental Figure 5, C and D). Importantly, miR-33a–overexpressing cells displayed a markedly enhanced ability for neurosphere formation compared with control cells (Figure 2E and Supplemental Figure 6J). We also performed single cell-tracing experiments right after lentiviral infection before miR-33a was overexpressed and found an almost 3-fold increase in the ability of single non-GICs to form neurospheres (Figure 2F), indicating that the observed enhancement in neurosphere formation was an intrinsic property conferred by miR-33a on CD133− non-GICs rather than the overgrowth of GICs within the impure non-GIC population isolated from tumor samples. Consistent with the increased neurosphere-formation capability, CD133− non-GICs overexpressing miR-33a also expressed higher levels of stemness-associated genes, including nestin, *OLIG2*, and *BMI1* (Figure 2G). Interestingly, the morphology of miR-33a–overexpressing cells was transformed to one with sphere-like cell aggregates that was less attached to the culture dish, in sharp contrast with the control cells, which displayed a dispersed morphology and attached normally to the culture dish (Figure 2H). The most important cri-

terion for the functionally defined GICs is their potent ability to initiate tumor formation in immune-compromised mice, so we next examined whether miR-33a could affect the tumor-initiating ability of the non-GICs. As shown in Figure 2I, intracranial tumors initiated by the CD133$^-$ non-GICs with miR-33a overexpression progressed faster than the vector control cells. Together, these results indicate that CD133$^-$ non-GICs stably expressing miR-33a could display features closely resembling CD133$^+$ GICs as a consequence of reprogramming of those cells into a GIC-like state.

PDE8A and UVRAG are direct targets of miR-33a. Potent effects of miR-33a in maintaining the self-renewal of GICs and reprogramming non-GICs prompted us to explore the downstream effectors of miR-33a. In an effort to determine the potential downstream mRNA targets regulated by miR-33a, we integrated mRNA expression profiling with bioinformatic predictions. Using microarray technology, we generated a list of downregulated genes (0.8-fold threshold) in miR-33a–overexpressing D456MG cells. Further analysis of the microarray data indicated that miR-33a overexpression caused a significant preferential downregulation of predicted miR-33a targets (Supplemental Figure 9). Overlapping this list with the candidate list produced by 3 prediction algorithms, including PicTar, TargetScan, and microRNA.org, we narrowed the miR-33a target candidates down to a total of 90 genes. We further verified the mRNA expression level of each candidate on this 90-gene list by qRT-PCR in non-GICs as defined by their CD133$^-$ status isolated from D456MG and 11-0040 lines overexpressing miR-33a. This round of screening yielded 18 putative mRNA candidates that were significantly and consistently downregulated by miR-33a overexpression in both glioma lines, which are listed in Supplemental Table 3. It is possible that expression of some of the 18 candidate genes may be regulated by miR-33a indirectly. To further narrow down these candidates that are most likely to be direct targets of miR-33a, we employed AGO-2 antibody to pull down RNAs associated with RNA-induced silencing complex (RISC) to identify mRNAs selectively enriched in RISC after miR-33a overexpression by qRT-PCR (Figure 3, A and B). As an internal positive control, miR-33a incorporation into RISC was increased around 30-fold in miR-33a overexpression cells (Figure 3C). We then examined those candidate genes that do contain miR-33a seed sequences in their 3′ UTR and identified the mRNAs encoded by 2 genes, *PED8A* and *UVRAG*, with significantly elevated enrichment in miR-33a–overexpressing cells compared with the vector control group (Figure 3D). In addition, we examined several previously identified targets of miR-33a, including *ABCA1*, *ABCG1*, *CROT*, *CPT1A*, *PRKAA1*, *IRS1*, and *IRS2*, but found little or only modest increases in the level of these mRNAs incorporated into RISC, as determined by this assay (Figure 3D). These data suggest that miRNAs suppress their targets in a context-dependent manner. Consequently, we focused on the determination of whether the elevated levels of mRNA for *PDE8A* and *UVRAG* detected in the RISC immunoprecipitation were correlated with decreased levels of their encoded protein products, using Western blot analysis on cell lysates derived from both GICs and non-GICs isolated from the same 2 GBM lines. As shown in Figure 3E, the protein levels of these 2 genes were indeed changed correspondingly when the status of miR-33a expression was manipulated in those cells. To further explore whether these 2 genes represent direct targets of miR-33a, we conducted luciferase reporter assays to determine whether the putative binding sites of miR-33a in the 3′ UTR of *PDE8A* and *UVRAG* (Supplemental Figure 10) are important for miR-33a–mediated suppression. Indeed, luciferase reporter expression was repressed by miR-33a in a dose-dependent manner in 293T cells for both constructs; whereas 3′ UTR with mutated miR-33a–binding sites of *PDE8A* and *UVRAG* was not (Figure 3F). Collectively, these data support the notion that PDE8A and UVRAG serve as direct targets of miR-33a in glioma cells.

Repression of PDE8A and UVRAG expression is required for miR-33a to maintain the biological properties of GICs. Since both PDE8A and UVRAG have never been implicated as playing roles in GBM progression, we first determined their relative levels of expression in CD133$^+$ GICs versus CD133$^-$ non-GICs and detected lower amounts of both proteins in CD133$^+$ GICs in comparison with CD133$^-$ non-GICs (Figure 4A). We then tested the effect of overexpressing these 2 genes in CD133$^+$ GICs, respectively (Supplemental Figure 11A). Consistent with their status as targets of miR-33a, their overexpression could recapitulate phenotypes of miR-33a knockdown in CD133$^+$ GICs, as demonstrated by the compromised neurosphere formation and growth in culture, and tumor progression in vivo (Supplemental Figure 11, C–E). Next, we used a lentiviral system to deliver 2 independent short-hairpin RNAs to stably knock down the expression level of PDE8A or UVRAG individually in non-GICs, respectively (Figure 4B and Supplemental Figure 11B) and determined whether either of them could enhance the ability of CD133$^-$ non-GICs to adapt a phenotype associated with CD133$^+$ GICs. As shown in Figure 4, C and D, and Supplemental Figure 11F, reducing the expression of either *PDE8A* or *UVRAG* could significantly augment the ability of CD133$^-$ non-GICs to form neurospheres and modestly increase their growth rate. Consistent with the change in their behavior to resemble that of the CD133$^+$ GICs, expression of several stemness markers was induced in CD133$^-$ non-GICs following the knockdown of PDE8A or UVRAG (Figure 4E). To further determine whether the observed phenotypic properties of CD133$^+$ GICs are attributed to the suppression of PDE8A and UVRAG by miR-33a, we tested whether reducing the expression of either *PDE8A* or *UVRAG* or both genes together could have an impact on the ability of CD133$^+$ GICs to form neurospheres when miR-33a is suppressed. Consistent with the notion that both genes act as critical effectors downstream from miR-33a, CD133$^+$ GICs with cosuppression of miR-33a and either of its targets showed enhanced, although not fully rescued, neurosphere formation and self-renewal ability compared with CD133$^+$ GICs bearing a scramble control shRNA for PDE8A or UVRAG and the miR-33a sponge. More importantly, double-knockdown of both genes showed a combined effect on neurosphere formation ability, suggesting that miR-33a's positive effect on GICs is dependent on suppressing both PDE8A and UVRAG. (Figure 4F). Similar phenotypes were also observed in a separate patient-derived xenograft glioma line 11-0040 (Supplemental Figure 11G). Together, these data indicate that miR-33a functions to control the biological property of CD133$^+$ GICs at least partially through repressing its direct targets PDE8A and UVRAG.

Both PKA- and NOTCH-signaling pathways are required by miR-33a to maintain the biological properties of GICs. Functional validation of *PDE8A* and *UVRAG* as critical effectors for miR-33a

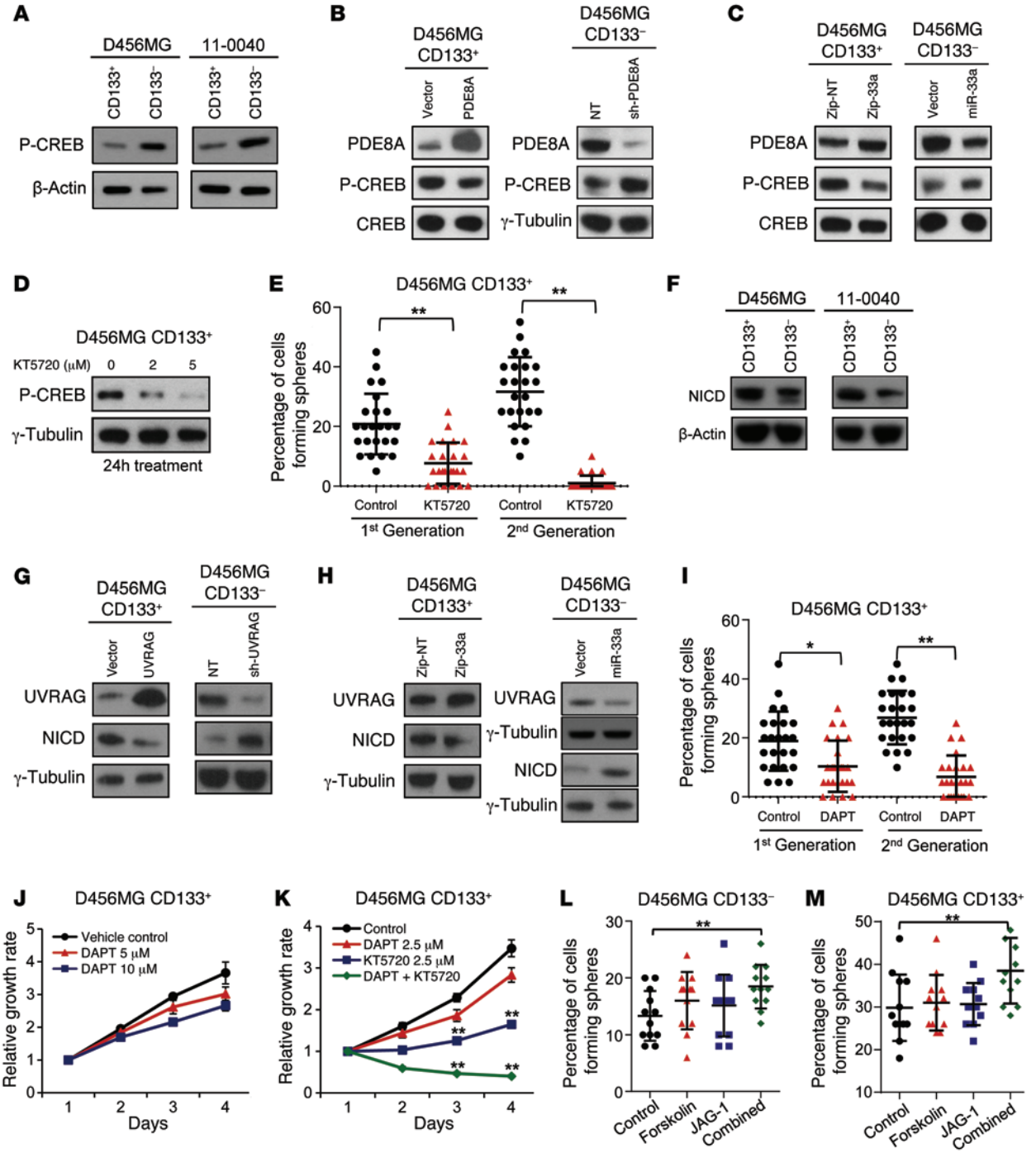

Figure 5. PDE8A and UVRAG regulate GIC self-renewal through the PKA and Notch pathways. (**A**–**C**) Immunoblotting was performed to show p-CREB levels in CD133$^+$ and CD133$^-$ glioma cells (**A**), PDE8A-overexpressing and -knockdown D456MG cells (**B**), and D456MG cells with miR-33a reduction or overexpression (**C**). (**D**) Immunoblotting was performed to show p-CREB levels after 24-hour treatment of 2 μM and 5 μM KT5720 in CD133$^+$ D456MG cells. (**E**) Neurosphere formation assay was performed in CD133$^+$ D456MG cells incubated with 2 μM KT5720 or vehicle control. (**F**–**H**) Immunoblotting was performed to show NICD levels in CD133$^+$ and CD133$^-$ glioma cells (**F**), CD133$^+$ D456MG cells with UVRAG overexpression or knockdown (**G**), and D456MG cells with miR-33a suppression or overexpression (**H**). (**I**) Neurosphere formation assay was performed in CD133$^+$ D456MG cells incubated with 10 μM DAPT or vehicle control. (**J**) Growth rates of CD133$^+$ D456MG cells incubated with 0 μM, 5 μM, and 10 μM DAPT were measured by cell titer assay. (**K**) Growth rates of CD133$^+$ D456MG cells incubated with vehicle control, 2.5 μM DAPT, 2.5 μM KT5720, or their combination was measured by cell titer assay. (**L**) Neurosphere formation assay was performed in CD133$^-$ D456MG cells incubated with vehicle control, 2 μM forskolin, 0.2 μM JAG-1, or a combination of these reagents. (**M**) The same assays as in **L** were performed using CD133$^+$ D456MG cells, except 400 nM forskolin, 40 nM JAG-1, or their combination was utilized. For neurosphere formation assays, 50 cells were plated in each well of 24-well plates. $^*P < 0.05$; $^{**}P < 0.01$.

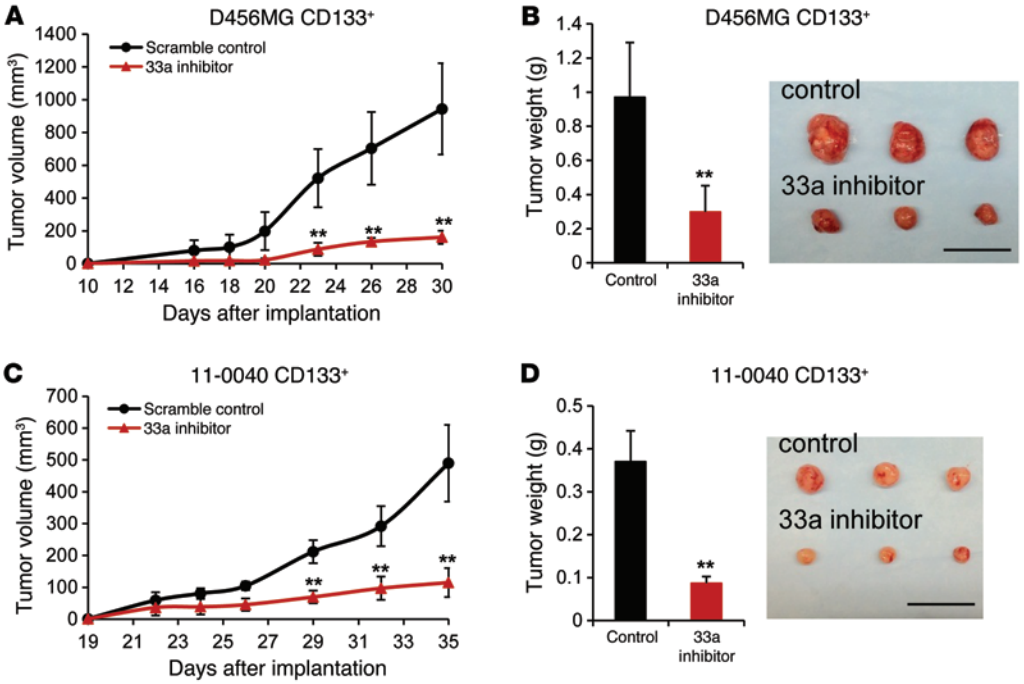

Figure 6. Treatment with a miR-33a LNA inhibitor suppressed tumor growth in vivo. (**A** and **C**) 100,000 D456MG or 11-0040 glioma cells were implanted subcutaneously into nude mice with 3 animals in each group. Treatment was started 10 days and 19 days after implantation of the 2 tumor lines, respectively. 5 μg LNA scramble control or miR-33a inhibitor was injected intratumorally into each subcutaneous tumor every other day. Tumor volumes were measured by a vernier caliper on the indicated days. (**B** and **D**) Subcutaneous tumors derived from D456MG and 11-0040 glioma cells in the control and miR-33a LNA inhibitor–treated group were weighted immediately after tumors were harvested. Pictures of subcutaneous tumors were displayed. Scale bars: 20 mm.

in CD133$^+$ GICs prompted us to explore how these 2 genes could mediate the function of miR-33a to control the biological properties of GICs. PDE8A belongs to a family of phosphohydrolases, which selectively catalyze the hydrolysis of cAMP (24), so this enzyme negatively regulates the cellular level of cAMP by controlling its degradation rate. We reasoned that the level of PDE8A could directly modulate the activity of the protein kinase A (PKA) pathway, which depends on cellular cAMP for its activation (25). To test this possibility, we examined the functional status of a canonical downstream effector of the PKA pathway, phosphorylated CREB (p-CREB) (26), which has a higher level in CD133$^+$ GICs compared with CD133$^-$ cells (Figure 5A). Overexpression of PDE8A in CD133$^+$ cells decreased the level of p-CREB, and knocking down of PDE8A in CD133$^-$ non-GICs increased the level of p-CREB (Figure 5B). Consistently, we observed reduced levels of p-CREB after miR-33a knockdown in CD133$^+$ GICs and elevated levels of p-CREB after miR-33a overexpression in CD133$^-$ non-GICs (Figure 5C). We also directly measured the levels of cAMP and observed its increase when miR-33a was overexpressed or PDE8A was knocked down in CD133$^-$ non-GICs, respectively (Supplemental Figure 12, A and B). In addition, we analyzed the microarray data of CD133$^-$ D456MG cells overexpressing miR-33a and found that a collection of 80 genes associated with the cAMP/PKA pathway displayed a significant preferential upregulation after miR-33a overexpression (Supplemental Figure 13A), indicating an increased activity of the cAMP/PKA pathway. Thus, these data indicated that miR-33a might promote self-renewal of CD133$^+$ GIC through increasing PKA activity. Since the PKA pathway has not been previously implicated as playing a role in stem cell biology, we further tested the functional relevance of the PKA pathway in GICs by utilizing a small molecule inhibitor of PKA, KT5720, to treat CD133$^+$ GICs. As expected, 2 μM KT5720 treatment efficiently blocked CREB phosphorylation in GICs (Figure 5D). Importantly, KT5720 significantly reduced neurosphere formation in CD133$^+$ GICs (Figure 5E). Taken together, these data strongly suggest that miR-33a promotes self-renewal of CD133$^+$ GICs by repressing its direct target, PDE8A, to enhance the activity of the PKA pathway.

UVRAG, the other target of miR-33a, has been reported as regulating autophagy (27) and chromosome stability (28, 29) and acting as a tumor suppressor because allelic mutation of UVRAG was found at high frequencies in human colon cancers and its ectopic expression in a colon cancer cell line resulted in decreased proliferation and xenograft tumor formation (30). We did not detect any alteration in the ratio of LC3 I/II in GICs or non-GICs where the level of miR-33a was manipulated (data not shown), indicating that miR-33a would not affect autophagy in the glioma cells. On the other hand, a separate report suggested that UVRAG could mediate NOTCH endocytosis to attenuate NOTCH signaling in regulating organ rotation during development in *Drosophila* (31). Since NOTCH has been shown previously to be critical for GIC self-renewal and resistance to radiotherapy (RT) (32), we hypothesized that UVRAG might represent a link between miR-33a and NOTCH signaling. As shown in Figure 5F, NOTCH intracellular domain (NICD), which is the cleaved and active domain of NOTCH acting as the effector of NOTCH by translocation into the nucleus, exhibited a higher level in CD133$^+$ GICs compared with CD133$^-$ cells. In CD133$^+$ GICs, we observed a decreased level of NICD following the overexpression of UVRAG (Figure 5G). Conversely, knocking down the expression of UVRAG led to an increased NICD level in non-GICs (Figure 5G), suggesting that UVRAG acts as an antagonist of the NOTCH pathway. Importantly, repressing miR-33a function also reduced NICD levels in CD133$^+$ GICs, indicating suppressed activity of the NOTCH pathway; on the other hand, overexpression of miR-33a in CD133$^-$ non-GICs promoted the activity of the NOTCH pathway, as indicated by an increase in the level of NICD (Figure 5H) and a significant preferential upregulation of 68 genes associated with the NOTCH pathway,

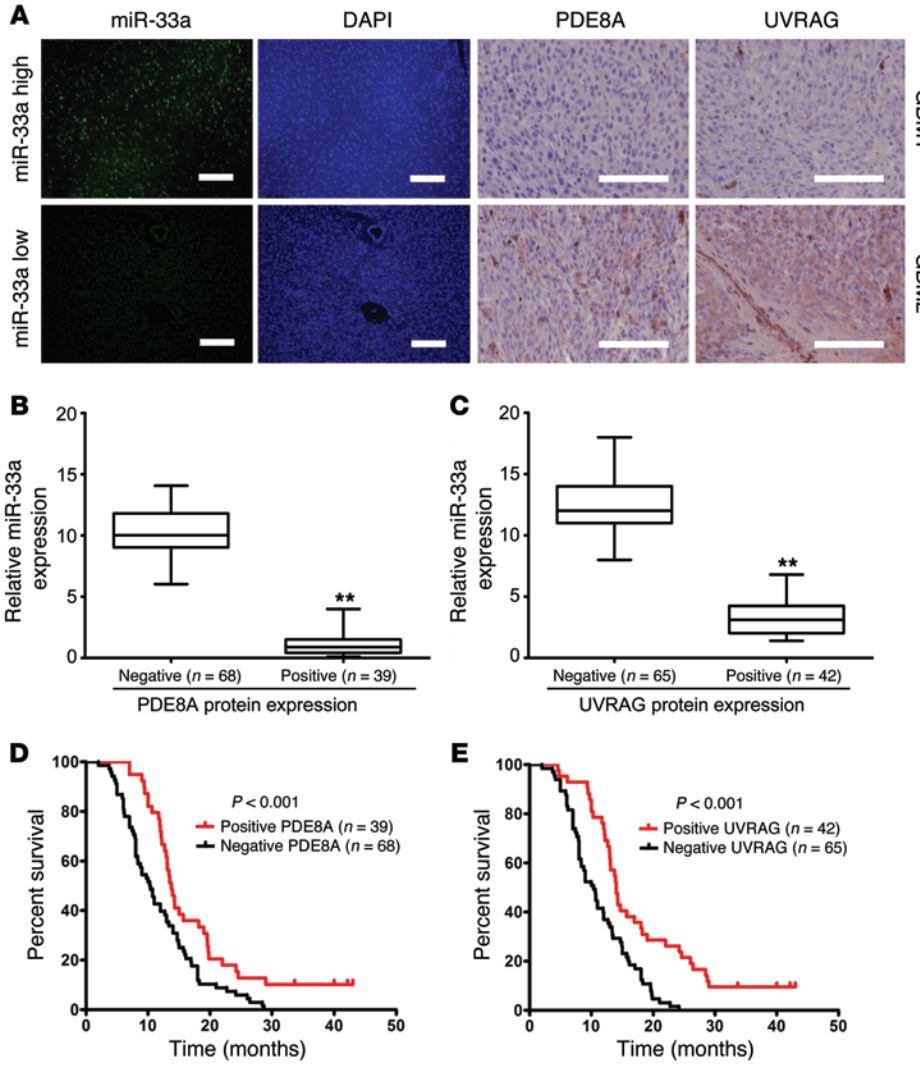

Figure 7. Clinical correlations between expression profiles of miR-33a, its 2 main targets, and GBM prognosis. (**A**) Representative images of ISH of miR-33a and IHC of PDE8A and UVRAG in the TMA of 107 GBM patient samples. Scale bars: 100 μm (ISH); 200 μm (IHC). (**B** and **C**) Correlation of the relative levels of miR-33a expression with the immunoreactivity of PDE8A and UVRAG protein in these GBM tumor tissues was quantified. (**D** and **E**) The IHC analysis of PDE8A (H) or UVRAG (I) was performed on 107 human GBM tumor tissues, and correlations between their expression levels and overall patient survival were shown by Kaplan-Meier curves. $^{**}P < 0.01$.

as measured by microarray analysis (Supplemental Figure 13B). In order to further investigate whether UVRAG functions to regulate NOTCH signaling through affecting NOTCH transcription or NICD cleavage, the mRNA level of *NOTCH1* was determined, but we found no changes in CD133$^+$ GICs with miR-33a suppression or CD133$^-$ non-GICs overexpressing miR-33a (Supplemental Figure 14, A and B), suggesting that UVRAG most likely affects NOTCH signaling at the level of NICD activation. This notion was also supported by the microarray analysis showing that neither *NOTCH1* nor the other *NOTCH* genes were altered at their mRNA levels. We then examined the expression levels of the 4 essential subunits of γ-secretase, which is the enzyme responsible for NOTCH cleavage to generate NICD (33), and found none of these subunits displayed a consistent change in their mRNA levels when the level of miR-33a was altered (Supplemental Figure 14, C–F).

Employing a different approach to antagonize NOTCH signaling to further probe a role for UVRAG in regulating NOTCH signaling, we added DAPT, a γ-secretase inhibitor, to the CD133$^+$ D456MG cells and found the self-renewal of those cells to be significantly suppressed (Figure 5I), but with only a modest effect on the growth rate of the same cells (Figure 5J). Thus, the NOTCH antagonist DPAT acted in the same manner as the overexpression of UVRAG, which countered the reported NOTCH function in supporting GIC self-renewal. We also took advantage of the availability of these small molecule inhibitors to assess the combinational effect of simultaneously blocking PKA and NOTCH pathways by adding KT5720 and DAPT together to the GICs. As shown in Figure 5K, the growth of CD133$^+$ D456MG cells was dramatically inhibited by the combined action of these 2 inhibitors in comparison with the addition of KT5720 or DAPT separately.

Finally, we tested whether enhancing the activities of both PKA and NOTCH pathways in CD133$^-$ non-GIGs could induce a phenotype associated with GICs. We treated CD133$^-$ D456MG cells with Forskolin, an agonist for the cAMP/PKA pathway, and JAG-1, a ligand to activate NOTCH signaling. While a low level of either agent alone displayed little activity to increase the ability of those CD133$^-$ non-GIGs to form neurospheres, combinational treatment of those cells with the agonists for both pathways led to a synergistic effect, indicating that simultaneous activation of these 2 pathways is needed to confer the self-renewal capability on to the CD133$^-$ non-GIGs (Figure 5L). This positive effect from treatment with the agonists for the 2 pathways was also observed in CD133$^+$ D456MG cells (Figure 5M). Taken together, these results strongly suggest that 2 independent pathways, PKA and NOTCH,

act cooperatively as effectors of miR-33a to positively regulate the biological properties of GICs.

Targeted inhibitor of miR-33a suppressed tumor formation in vivo, and the expression profiles of miR-33a and its 2 target genes are inversely correlated in GBM specimens. Since our functional assays have demonstrated the indispensability of miR-33a in maintaining the biological properties of GICs and GIC-derived GBM progression, we tested whether blocking miR-33a activity could have potential therapeutic value. To achieve this goal, we employed a modified small RNA inhibitor (locked nucleic acid [LNA]) of miR-33a to treat nude mice bearing subcutaneous xenografts initiated by D456MG or 11-0040 glioma cells, since the LNA in its current form was unable to penetrate the blood-brain barrier (data not shown). Following a regimen of administering the inhibitor every other day for 30 to 35 days, the mice were sacrificed and tumors removed for analysis. As displayed in Figure 6, A–D, in comparison with the control groups, treatment with the miR-33a–LNA caused significant decreases in the growth rates and weights of tumors inoculated with GICs derived from the 2 xenografted glioma lines. We also validated that the protein levels of the 2 identified targets of miR-33a, PDE8A and UVRAG, were upregulated after treatment of the miR-33a inhibitor both in vitro (Supplemental Figure 15A) and in the subcutaneous xenografts (Supplemental Figure 15, B and C), indicating the specificity of the miR-33a inhibitor. To evaluate the potential of the miR-33a–controlled signaling network as a therapeutic target in GBM, we conducted analysis on the TMAs and demonstrated that protein levels of PDE8A and UVRAG were inversely correlated with the relative levels of miR-33a expression measured by ISH in those GBM samples (Figure 7, A–C; a scramble ISH control for detecting miR-33a expression was also included in the Supplemental Figure 16). Finally, we investigated the clinical relevance between prognosis of GBM patients with *PDE8A* or *UVRAG* using the same TMA as for the miR-33a analysis and found significant correlations in the expression profiles of both genes with the clinical outcome of those patients (Figure 7, D–E). Taken together, the results of these proof-of-concept experiments, as well as the correlated expression profiles of mir-33a and its 2 target genes in GBM specimens with patient prognosis, lend further support to our conclusion that the miR-33a–mediated signaling pathway is critical for GBM tumor progression and that targeting this signaling network could be a potentially effective therapeutic strategy against GBM in the future.

Discussion

A miRNA controls biological properties of GICs. A decade has passed since the discovery of GICs, or glioma stem cells, among the heterogeneous population of tumor cells within the GBM tumor mass using the cell-surface marker CD133. Subsequently, it became clear that glioma cells without the expression of CD133 could also possess the same properties defined functionally to be associated with GICs, as GICs could be enriched by a different cell surface marker, SSEA-1, or via culturing the glioma cells dispersed from tumor mass under specified conditions. Although lingering doubts persist regarding the importance or even existence of GICs in the context of GBM, extensive research has been done to demonstrate their critical roles in GBM initiation, progression, and recurrence associated with resistance to radio- and chemotherapy. However, almost all of those studies have centered on the biological properties of the GICs, without providing much information on the features of their counterparts within the tumor mass, namely those non-GICs, probably due to the technical difficulty in separating the GICs from the rest of the tumor cell population. To fill this significant gap in our knowledge on the molecular basis that distinguishes GICs from non-GICs, we have, in the present study, focused on the identification and functional characterization of the signaling network that controls the identity of GICs. To this end, we have generated compelling evidence to support the notion that a single miRNA, miR-33a, sits at the center of a signaling network, since changes in its expression pattern could drastically alter the biological properties of GICs and non-GICs. The higher level of miR-33a expression in GICs appears to be required to maintain the primary biological features of those cells, including self-renewal, stemness, and tumor initiation in vivo. In other words, the pluripotent-like signature displayed by GICs could therefore be at least partially attributed to the upregulation of miR-33a. Moreover, we have provided evidence that miR-33a possesses the capability to reprogram non-GICs with differentiated features to resemble GIC-like status. In a broad sense, miR-33a, together with the miR-302/367 cluster, miR-34, and let-7 family that could regulate the reprogramming of iPS cells or neural stem-cell commitment (34–36), appears to belong to an elite group of miRNAs that can function as "master determinants" for controlling the signaling network associated with determination of cell fate and identity. The newly established status of miR-33a as an oncomir is also consistent with the findings that higher expression levels of miR-33a are correlated with poor survival of GBM patients.

The requirement of activities from 2 pathways to maintain the properties of GICs. Because of their potential to target multiple genes, miRNAs are believed to exert their regulatory effects on specific biological processes through fine-tuning the activities of multiple signaling pathways or networks. In this case, it was not surprising that we have identified at least 2 downstream effectors, *PDE8A* and *UVRAG*, that both serve as direct targets for miR-33a to regulate the activities of 2 major signaling pathways in GICs. While the NOTCH pathway has been reported to be important for GIC maintenance and tumor initiation, our finding is the first demonstration, to our knowledge, of the critical role for UVRAG in suppressing the self-renewal program of GICs as an antagonist of NOTCH through its regulation of NOTCH endocytosis. Moreover, this finding has also provided an alternative explanation for UVRAG to be defined as a tumor suppressor in the context of cancer, since we did not observe any changes in the autophagy activity in glioma cells when UVRAG expression was altered (data not shown). In contrast with the NOTCH pathway, virtually nothing has been known about the function of the cAMP/PKA pathway in cancer stem cell regulation until we revealed here the critical role of PDE8A as a potent negative regulator of the biological properties of GICs. Although we have shown that inhibiting PDE8A expression by miR-33a increased the level of cAMP and significantly enhanced PKA activity, as measured by the phosphorylation of its known substrate CREB transcription factor, the exact activities of the cAMP/PKA at the mechanistic level in regulating GIC function remain to be further investigated.

The finding that miR-33a represses both PDE8A and UVRAG to enhance the activities of the cAMP/PKA and Notch pathways

exemplifies how miRNAs, which often have only mild to modest repressive effects on single target genes, could produce dramatic biological outcomes. The widespread distribution of their targeting sequences throughout the genome has predetermined the unique mechanism of their working mode, which is to orchestrate modest changes in the expression pattern of groups of genes to produce convergent effects from multiple pathways or signaling networks. This notion is clearly demonstrated by the synergistic effects of the combined actions of either agonists or antagonists for both PKA and NOTCH pathways in conferring the self-renewal property on non-GIGs or blocking the growth of GICs and supported by the clinical evidence that the expression profiles of miR-33a and its 2 targets are inversely correlated in GBM specimens and patient prognosis.

A potential therapeutic avenue for GBM. A rapidly growing body of evidence has shown miRNAs as potential targets for cancer therapy. For example, overexpression of miR-26 by adenoassociated virus in a MYC-driven liver cancer model can attenuate tumor formation (37); inhibition of miR-10b by delivery of miRNA antagonists does not block primary tumor growth, but can attenuate breast cancer metastasis in animal models (38). The chemical structure of miRNA offers extraordinary target specificity for miRNA-based therapeutic development. Chemically locked miRNA mimetics, by avoiding the risk of introducing foreign DNA molecules into the body, provide extra safety and stability in vivo when developed as potential anticancer drugs. In our study, LNA inhibitor of miR-33a was able to block tumor progression in a xenograft model, providing a promising approach to combatting malignant gliomas, particularly those driven by GICs. Although systemic delivery of LNA inhibitors into the brain crossing the blood-brain barrier remains challenging, the striking inhibitory effect of miR-33a antagonists on subcutaneous tumor growth strongly suggests that further efforts toward development of anti–miR-33a–based therapeutics are fully warranted.

Methods

Isolation of GICs and non-GICs from patient specimens and mice xenografts. Patient specimens were collected from the Duke Brain Tumor Center during 2011 and 2012. Fresh patient specimens were dissociated by the Papain Dissociation System (Worthington Biochemical) according to the manufacturer's instructions. GICs were enriched by culturing cells in Neurobasal medium (Invitrogen) supplemented with B27 (without vitamin A from Invitrogen), L-glutamine (Invitrogen), sodium pyruvate (Invitrogen), 10 ng/ml bFGF, and 10 ng/ml EGF (Millipore); non-GICs cells were cultured in Improved MEM Zinc Option (Invitrogen) with 10% FBS. Human D456MG cell line or primary patient specimens were passaged in immunocompromised athymic BALB/c nu/nu mice as subcutaneous xenografts in accordance with a protocol approved by the Duke University Institutional Animal Care and Use Committee, and cells were yielded by dissociation of xenografts as described above. To enrich GICs by the marker CD133, cells were separated by microbead-conjugated CD133 antibodies and magnetic columns (Miltenyi Biotec). $CD133^+$ cells were designated as GICs and cultured in Neurobasal medium described above; $CD133^-$ cells were designated as non-GICs and cultured in Improved MEM Zinc Option with 10% FBS. To enrich GICs by the marker SSEA-1, cells were stained by FITC-conjugated SSEA-1 antibody (eBioscience) and separated by flow cytometry. Prior to experiments, non-GICs were cultured in Neurobasal medium for at least 12 hours so that all functional experiments for all types of cells were performed in identical media.

miRNA profiling. Total RNA was prepared using the mirVana miRNA Isolation Kit (Ambion). miRNA was reverse transcribed into cDNA by RT^2 miRNA First Strand Kit (QIAGEN), and profiling was performed using RT^2 miRNA PCR Array (QIAGEN), which simultaneously profiled 88 different human miRNAs with potential roles in cell self-renewal and differentiation. Human small nuclear U6 RNA was amplified as a normalization control. The profiling and analysis was performed using a Mastercycler Realplex system (Eppendorf).

Neurosphere formation assay. GICs, non-GICs, normal, or transformed human astrocytes with indicated modification or treatment were plated in 24-well plates at indicated cell numbers per well by flow cytometry with 1 ml of the same medium used for the GICs described earlier. After 7 to 10 days, the number of neurospheres in each well was quantified. Then spheres were dissociated to single cells and plated again in 24-well plates at indicated cell numbers per well by flow cytometry to form a second generation of neurospheres.

Isolation of RISC-associated RNA. Following a previously published procedure (39), 10 million 11-0040 $CD133^-$ cells with miR-33a overexpression or vector control were lysed in 750 μl 1× PXL buffer (1× PBS with 0.1% SDS, 0.5% sodium deoxycholate, and 0.5% NP-40 substitute) with proteinase inhibitor (P2714; Sigma-Aldrich) and 0.3 U/μl SUPERase•In RNase Inhibitor (Life Technologies). Lysates were cleared by centrifugation at 13,793 *g* for 15 minutes. For each sample, 50 μl Dynabeads Protein A (Invitrogen) was incubated with 15 μg rabbit anti-mouse IgG (Jackson ImmunoResearch) for 45 minutes at room temperature, then washed with 500 μl 1× PBS 3 times. Then 15 μl Anti-pan Ago, clone 2A8 antibody (Millipore), or the same amount of mouse IgG (Jackson ImmunoResearch) was added to the beads for 2 hours at 4°C. Beads were washed twice with 500 μl 1× PXL, and cell lysates were added and incubated for another 2 hours at 4°C. All immunoprecipitation samples were washed 3 times with 500 μl 1× PXL buffer. The immunoprecipitated RNA was released by proteinase K digestion and extracted by phenol/chloroform/isopropyl alcohol. RNA was pelleted by ethanol precipitation with glycogen, resolved, and treated with DNase I (New England BioLabs).

LNA miR-33a inhibitor treatment. LNA miR-33a inhibitor (TGCAACTACAATGCA) and a LNA scramble control (ACGTCTATACGCCCA) were synthesized by Exiqon. Subcutaneous transplantation of glioma cells into athymic BALB/c nu/nu mice was performed in accordance with a protocol approved by the Duke University Institutional Animal Care and Use Committee. After subcutaneous tumors became visible with the naked eye, mice were randomized into 2 groups for treatment: scramble control and miR-33a inhibitor. Mice were treated with 5 μg per mouse LNA oligonucleotide packaged with MaxSuppressor In vivo RNA-LANCEr II (Bio Scientific) intratumorally every 2 days. At the same time, tumor size was measured every 2 or 3 days by calipers, and tumor volume was calculated as $V\ (mm^3) = L \times W^2 \times 0.5$ (where V indicates volume, L indicates length, and W indicates width) until tumors were harvested and weighted immediately after sacrificing the mice.

ISH and IHC staining in GBM TMAs. TMA included a total of 107 paraffin-embedded GBM tissues, which had been clinically and histopathologically diagnosed at the Department of Neurosurgery, the Second and Fourth Affiliated Hospitals of Harbin Medical University (Harbin, China), from 2002 to 2007. The histological features of all the

specimens were confirmed by pathologists according to WHO criteria. None of the patients had received RT or chemotherapy before tumor resection. The correlations between the expression levels of miR-33a and clinical parameters are displayed in Supplemental Table 4.

ISH was used to evaluate the expression of miR-33a using a miR-33a probe from RiboBio (Cy3 labeled). The signals of ISH of tissue sections were examined and scored separately by 2 independent investigators blinded to the histopathological features and patient data of the samples. miR-33a expression was evaluated according to the proportion of positively stained tumor cells and the intensity of staining. The proportion of positively stained tumor cells was graded as follows: 0, no positive tumor cells; 1, 0.01%–25% positive tumor cells; 2, 25.01%–50% positive tumor cells; 3, 50.01%–75% positive tumor cells; 4, 75% or greater positive tumor cells. The cells at each intensity of staining were recorded on a scale of 0 (no signal), 1 (weak), 2 (moderate), and 3 (strong). The hybridization score for each section was computed by the following formula: hybridization score = staining intensity × proportion of positively stained tumor cells. A total score of 0–12 was calculated and graded as negative (–, score: 0), weak (+, score: 1–4), moderate (++, score: 5–8), or strong (+++, score: 9–12). Cutoff values to define the high and low expression of miR-33a were chosen on the basis of a measurement of heterogeneity with the log-rank test statistic with respect to overall survival. Because the optimal cutoff thresholds were identified from the current study as 5, a hybridization score of 5 or more was taken to define tumors as high expression, and a hybridization score of less than 5 to define tumors as low expression of miR-33a. The quantification of immunohistochemical staining of PDE8A and UVRAG was performed in the same manner as for miR-33a. PDE8A and UVRAG antibodies were purchased from LifeSpan Biosciences Inc., and IHC was carried out according to the manufacturer's instructions.

Statistics. Results are reported as mean ± SEM. Significance was tested by 2-tailed Student's *t* test using GraphPad Prism software or 1-way ANOVA for multiple comparisons. Significance of Kaplan-Meier curves was determined by log-rank (Mantel-Cox) test using GraphPad Prism software. A *P* value of less than 0.05 was considered significant.

Study approval. The GBM TMA study was approved by the institutional review board and the ethics committee of Harbin Medical University, and written informed consent was obtained from all patients. GBM patient samples were obtained from Duke University Brain Tumor Tissue Bank. The study was approved by the institutional review board of Duke University. Informed consent was obtained from all patients. All animal studies were approved by the institutional review board of Duke University.

Accession number. All original microarray data were deposited in the NCBI's Gene Expression Omnibus (GEO GSE59484).

Please refer to the Supplemental Methods section for more detailed information.

Acknowledgments

We thank M. Cook and B. Li for assistance with flow cytometry, D. Satterfield, B. Wiener, and L. Ehinger for assistance with collecting fresh GBM patient specimens, and the Duke Microarray Facility for assistance with microarray and data analysis. We thank the laboratories of Didier Trono and Eric Campeau for providing us with plasmids via Addgene. This work was supported by NIH grants (CA164791 to X-.F. Wang; AI091878 to Q.-J. Li); the National Natural Science Foundation of China (81201978 and 81200362), the Natural Science Foundation of Jiangsu Province (BK2012483), the Program for Advanced Talents within Six Industries of Jiangsu Province (2012-WSN-019), the Program for Development of Innovative Research Team in the First Affiliated Hospital of Nanjing Medical University, and the Priority Academic Program Development of Jiangsu Higher Education Institutions (to Huibo Wang). The Duke University Brain Tumor Tissue Bank is supported by the Duke University Brain Cancer SPORE.

Address correspondence to: Xiao-Fan Wang, Duke University School of Medicine, C218 LSRC, Box 3813, Durham, North Carolina 27710, USA. Phone: 919.681.4861; E-mail: xiao.fan.wang@duke.edu.

1. Central Brain Tumor Registry of the United States. *Statistical Report: Primary Brain Tumors in the United States, 1998–2002*. Hinsdale, Illinois, USA: CBTRUS; 2005.
2. Singh SK, et al. Identification of human brain tumour initiating cells. *Nature*. 2004;432(7015):396–401.
3. Yuan X, et al. Isolation of cancer stem cells from adult glioblastoma multiforme. *Oncogene*. 2004;23(58):9392–9400.
4. Liu G, et al. Analysis of gene expression and chemoresistance of CD133+ cancer stem cells in glioblastoma. *Mol Cancer*. 2006;5:67.
5. Bao S, et al. Glioma stem cells promote radioresistance by preferential activation of the DNA damage response. *Nature*. 2006;444(7120):756–760.
6. Bushati N, Cohen SM. microRNA functions. *Annu Rev Cell Dev Biol*. 2007;23:175–205.
7. Baek D, Villen J, Shin C, Camargo FD, Gygi SP, Bartel DP. The impact of microRNAs on protein output. *Nature*. 2008;455(7209):64–71.
8. Farazi TA, Spitzer JI, Morozov P, Tuschl T. miRNAs in human cancer. *J Pathol*. 2011;223(2):102–115.
9. Mendell JT. miRiad roles for the miR-17-92 cluster in development and disease. *Cell*. 2008;133(2):217–222.
10. Poliseno L, et al. Identification of the miR-106b~25 microRNA cluster as a proto-oncogenic PTEN-targeting intron that cooperates with its host gene MCM7 in transformation. *Sci Signal*. 2010;3(117):ra29.
11. Jazbutyte V, Thum T. MicroRNA-21: from cancer to cardiovascular disease. *Curr Drug Targets*. 2010;11(8):926–935.
12. Schraivogel D, et al. CAMTA1 is a novel tumour suppressor regulated by miR-9/9* in glioblastoma stem cells. *EMBO J*. 2011;30(20):4309–4322.
13. Chan XH, et al. Targeting glioma stem cells by functional inhibition of a prosurvival oncomiR-138 in malignant gliomas. *Cell Rep*. 2012;2(3):591–602.
14. Chen R, et al. A hierarchy of self-renewing tumor-initiating cell types in glioblastoma. *Cancer Cell*. 2010;17(4):362–375.
15. Ernst A, et al. De-repression of CTGF via the miR-17-92 cluster upon differentiation of human glioblastoma spheroid cultures. *Oncogene*. 2010;29(23):3411–3422.
16. Gerin I, et al. Expression of miR-33 from an SREBP2 intron inhibits cholesterol export and fatty acid oxidation. *J Biol Chem*. 2010;285(44):33652–33661.
17. Rayner KJ, et al. MiR-33 contributes to the regulation of cholesterol homeostasis. *Science*. 2010;328(5985):1570–1573.
18. Davalos A, et al. miR-33a/b contribute to the regulation of fatty acid metabolism and insulin signaling. *Proc Natl Acad Sci U S A*. 2011;108(22):9232–9237.
19. Son MJ, Woolard K, Nam DH, Lee J, Fine HA. SSEA-1 is an enrichment marker for tumor-initiating cells in human glioblastoma. *Cell Stem Cell*. 2009;4(5):440–452.
20. Suva ML, et al. Reconstructing and reprogramming the tumor-propagating potential of glioblastoma stem-like cells. *Cell*. 2014;157(3):580–594.
21. Ebert MS, Neilson JR, Sharp PA. MicroRNA sponges: competitive inhibitors of small RNAs in mammalian cells. *Nat Methods*. 2007;4(9):721–726.
22. Sonoda Y, et al. Formation of intracranial tumors by genetically modified human astrocytes defines four pathways critical in the development

of human anaplastic astrocytoma. *Cancer Res*. 2001;61(13):4956–4960.
23. Tabu K, et al. Analysis of an alternative human CD133 promoter reveals the implication of Ras/ERK pathway in tumor stem-like hallmarks. *Mol Cancer*. 2010;9:39.
24. Fisher DA, Smith JF, Pillar JS, St Denis SH, Cheng JB. Isolation and characterization of PDE8A, a novel human cAMP-specific phosphodiesterase. *Biochem Biophys Res Commun*. 1998;246(3):570–577.
25. Skålhegg BS, Taskén K. Specificity in the cAMP/PKA signaling pathway. differential expression, regulation, and subcellular localization of subunits of PKA. *Front Biosci*. 1997;2:d331–d342.
26. Sands WA, Palmer TM. Regulating gene transcription in response to cyclic AMP elevation. *Cell Signal*. 2008;20(3):460–466.
27. Liang C, Feng P, Ku B, Oh BH, Jung JU. UVRAG: a new player in autophagy and tumor cell growth. *Autophagy*. 2007;3(1):69–71.
28. Zhao Z, et al. A dual role for UVRAG in maintaining chromosomal stability independent of autophagy. *Dev Cell*. 2012;22(5):1001–1016.
29. Knaevelsrud H, et al. UVRAG mutations associated with microsatellite unstable colon cancer do not affect autophagy. *Autophagy*. 2010;6(7):863–870.
30. Liang C, et al. Autophagic and tumour suppressor activity of a novel Beclin1-binding protein UVRAG. *Nat Cell Biol*. 2006;8(7):688–699.
31. Lee G, Liang C, Park G, Jang C, Jung JU, Chung J. UVRAG is required for organ rotation by regulating Notch endocytosis in Drosophila. *Dev Biol*. 2011;356(2):588–597.
32. Wang J, et al. Notch promotes radioresistance of glioma stem cells. *Stem Cells*. 2010;28(1):17–28.
33. Kopan R, Ilagan MXG. γ-secretase: proteasome of the membrane? *Nat Rev Mol Cell Biol*. 2004;5(6):499–504.
34. Anokye-Danso F, et al. Highly efficient miRNA-mediated reprogramming of mouse and human somatic cells to pluripotency. *Cell Stem Cell*. 2011;8(4):376–388.
35. Choi YJ, et al. miR-34 miRNAs provide a barrier for somatic cell reprogramming. *Nat Cell Biol*. 2011;13(11):1353–1360.
36. Rybak A, et al. A feedback loop comprising lin-28 and let-7 controls pre-let-7 maturation during neural stem-cell commitment. *Nat Cell Biol*. 2008;10(8):987–993.
37. Kota J, et al. Therapeutic microRNA delivery suppresses tumorigenesis in a murine liver cancer model. *Cell*. 2009;137(6):1005–1017.
38. Ma L, et al. Therapeutic silencing of miR-10b inhibits metastasis in a mouse mammary tumor model. *Nat Biotechnol*. 2010;28(4):341–347.
39. Chi SW, Zang JB, Mele A, Darnell RB. Argonaute HITS-CLIP decodes microRNA-mRNA interaction maps. *Nature*. 2009;460(7254):479–486.